Assessing historical variability of South Asian monsoon lows and depressions with an optimized tracking algorithm

S. Vishnu[1], W. R. Boos[1,2], P. A. Ullrich[3], T. A. O'Brien[4,2]

[1]Department of Earth and Planetary Science, University of California, Berkeley, Berkeley, California, USA
[2]Climate and Ecosystem Sciences Division, Lawrence Berkeley National Laboratory, Berkeley, California, USA
[3]Department of Land, Air, and Water Resources, University of California, Davis, Davis, California, USA
[4]Earth and Atmospheric Sciences Department, Indiana University, Bloomington, Indiana, USA

Key Points:

- An objective, optimal algorithm for tracking monsoon low pressure systems is developed and applied to five reanalyses
- Climatological statistics of the resulting track datasets are consistent across reanalyses and comparable to two manually derived datasets
- Uncertainty analyses show that previously reported trends in Indian monsoon depressions may be artifacts of changes in the observing network

Corresponding author: S. Vishnu, `vishnus@berkeley.edu`

Abstract

Cyclonic low-pressure systems (LPS) produce abundant rainfall in South Asia, where they are traditionally categorized as monsoon lows, monsoon depressions, and more intense cyclonic storms. The India Meteorological Department (IMD) has tracked monsoon depressions for over a century, finding a large decline in their number in recent decades, but their methods have changed over time and do not include monsoon lows. This study presents a fast, objective algorithm for identifying monsoon LPS in high-resolution datasets. Variables and thresholds used in the algorithm are selected to best match a subjectively analyzed LPS dataset while minimizing disagreement between four atmospheric reanalyses in a training period. The streamfunction of the 850 hPa horizontal wind is found to be the best variable for tracking LPS; it is less noisy than vorticity and represents the complete non-divergent wind, even when flow is not geostrophic. Using this algorithm, LPS statistics are computed for five reanalyses, and none show a detectable trend in monsoon depression counts since 1979. Both the Japanese 55-year Reanalysis (JRA-55) and the IMD dataset show a step-like reduction in depression counts when they began using geostationary satellite data, in 1979 and 1982 respectively; the 1958-2018 linear trend in JRA-55, however, is smaller than in the IMD dataset and its error bar includes zero. There are more LPS in seasons with above-average monsoon rainfall and also in La Niňa years, but few other large-scale modes of interannual climate variability are found to modulate LPS counts, lifetimes, or track length consistently across all reanalyses.

1 Introduction

Cyclonic low pressure systems (LPS) are the dominant synoptic-scale phenomena that bring rain to India and surrounding regions during the boreal summer monsoon season. With outer diameters near 2,000 km, these monsoon LPS typically form over the northern Bay of Bengal then propagate to the northwest over India during the subsequent several days (Mooley, 1973; Godbole, 1977; Sikka, 1978). Although these storms have weak surface winds of order 10 m s^{-1}, they produce abundant rainfall, with precipitation rates peaking at 3-5 cm day^{-1} in composite means and some storms producing 10-50 cm of rain along their tracks (Sanders, 1984; Sikka, 2006; Boos et al., 2015; Hunt et al., 2016). Monsoon LPS make a large contribution to the total summer monsoon rainfall of continental South Asia (Yoon & Chen, 2005) and have produced catastrophic floods there (Houze Jr et al., 2011).

Given the importance of monsoon LPS, there is great interest in studying the variability of these storms. The India Meteorological Department (IMD) has kept records on LPS since the late nineteenth century (India Meteorological Department, 2011). They traditionally categorized these storms by intensity, with the weakest systems called monsoon lows (surface wind speeds less than 8.5 m s^{-1} and mean sea level pressure (MSLP) at least 2 hPa lower than surrounding regions), stronger systems called monsoon depressions (wind speeds 8.5-13.5 m s^{-1} and MSLP anomalies 4-8 hPa), and even stronger vortices called deep depressions and cyclonic storms (the use of surface wind speed or surface pressure as a metric for categorization has varied over time (India Meteorological Department, 2011)). The historical IMD dataset includes only depressions and stronger storms, but Mooley and Shukla (1987) and Sikka (2006) produced a separate dataset of both lows and depressions by manually identifying LPS from hand-analyzed daily weather charts of the IMD. These datasets have been used in numerous studies of variations in the number of monsoon LPS. For example, the number of LPS forming each summer has been shown to be modulated by the El Niño-Southern Oscillation (ENSO) (Hunt et al., 2016), the Pacific Decadal Oscillation (PDO) (Vishnu et al., 2018), and the Indian Ocean Dipole (IOD) (Krishnan et al., 2011), all of which are also associated with interannual variations in the strength of the mean Indian summer monsoon.

Based on the two track datasets just discussed, numerous studies have reported a large decrease in the number of monsoon depressions forming each summer in recent decades, together with an increase in the number of monsoon lows (Rajendra Kumar & Dash, 2001; Prajeesh et al., 2013; Vishnu et al., 2016, and reference therein). When characterized as a linear trend, the decrease in depression counts amounts to a reduction of around one per decade, from a mid-twentieth century value of about seven, although much of the decrease occurred as a step-wise reduction in the early 1980s (Vishnu et al., 2016). The years 2002, 2010, and 2012 contained the first summers, in over a century of record-keeping by IMD, with no monsoon depressions. The reduction in depression counts has been argued to be associated with a decrease in total summer rainfall in east-central India, the region of highest LPS track density (Vishnu et al., 2016). A decrease in overall LPS activity, including that of both lows and depressions, has been projected for the coming century as global mean temperature increases and the large-scale, seasonal mean monsoon circulation weakens (Sandeep et al., 2018; Rastogi et al., 2018). This projected decrease is accompanied by a poleward shift in the region of LPS genesis in next-century simulations using one global climate model (Sandeep et al., 2018), but the connection of such greenhouse gas-forced changes to past trends remains unclear, especially given the possible dominance of aerosol forcings in historical trends of mean monsoon strength (Ramanathan et al., 2005; Bollasina & Nigam, 2009).

The existence of a large trend in monsoon depression counts was questioned by Cohen and Boos (2014), who showed that no such trend could be detected in two reanalyses when automated algorithms were used to track and classify low-level vorticity and MSLP anomalies. Furthermore, Cohen and Boos (2014) found depression-strength LPS in those reanalyses during the years when IMD recorded none (2002, 2010 and 2012), and showed that satellite scatterometer data validated the intensity of the peak surface wind speeds near the centers of those particular storms. They also showed that there was no detectable trend in a satellite scatterometer record of synoptic-scale wind events over the Bay of Bengal, although that record extended back to only 1987. All of this raises numerous questions: are the two reanalyses examined by Cohen and Boos (2014) reliable tools for assessing trends in monsoon LPS, especially given that they extended back to only 1979, a few years before the step-wise reduction in IMD's depression counts? Should we expect trends inferred from the IMD record of depression counts to be unbiased, given the large changes since the late 19th century in the observing network, in methods used by IMD for identifying and classifying LPS, and possibly in practices used for creating the hand-drawn IMD weather charts?

All of this would seem to call for a reanalysis of monsoon LPS track datasets, analogous to the large international efforts to improve track datasets of past tropical cyclones (Landsea et al., 2008; Hagen et al., 2012; Landsea et al., 2014; Delgado et al., 2018). This would be a massive undertaking, made more difficult by the fact that IMD synoptic charts are not readily available and by the fact that monsoon LPS have weak circulations compared to tropical cyclones. Furthermore, the wind maxima of LPS are typically elevated a few kilometers above the surface (Godbole, 1977), rendering their identification and categorization using maps of MSLP even more difficult. Here we take an alternate approach by devising an algorithm that can identify LPS using elevated winds as well as surface conditions as represented in five atmospheric reanalyses, including the most modern ones that represent climate forcings and that extend back in time to the 1950s. This does not eliminate bias that might be introduced by the temporal evolution of the observing network on which those reanalyses are based, and, indeed, we demonstrate that step-wise changes in depression counts coincide with dates on which geostationary satellite imagery begin to be incorporated into the atmospheric state estimates.

This study builds on previous attempts to compile LPS track datasets from reanalyses (Hurley & Boos, 2015; Praveen et al., 2015), but with greater attention paid to the optimality of the tracking algorithm, to uncertainty characterization, to separation of the datasets used for training and validation of the algorithm, and to application of the algorithm to a larger number of reanalyses and to more modern reanalyses. Past efforts to track LPS in atmospheric reanalyses used the TRACK algorithm (Hodges, 1995, 1998; Hurley & Boos, 2015), which runs serially and requires degrading the underlying dataset to T42 spectral resolution (Thorncroft & Hodges, 2001; Manganello et al., 2019); both of those characteristics become problematic when working with modern atmospheric state estimates which often have horizontal grid spacings of 20-30 km. The algorithm we create for LPS identification builds on the TempestExtremes software (Ullrich & Zarzycki, 2017) and is thus fast, objective, and appropriate for high-resolution and variable grids. We hope to use this algorithm in future work to track monsoon LPS in large ensembles of high-resolution output from numerical weather prediction models and global climate models. In this study, the main focus is on constructing the algorithm, demonstrating its fidelity compared to existing, subjectively analyzed LPS datasets (Sikka, 2006), then examining the historical variability of LPS tracks on interannual and longer time scales.

2 Data and methods

2.1 Subjectively analyzed track datasets

We use two subjectively analyzed datasets of LPS tracks and intensities in the northern Indian Ocean. The first was compiled by Sikka (2006) and Mooley and Shukla (1987) and runs from 1888-2003, for the months of June through September. We hereafter refer to this as the Sikka archive. As mentioned in the Introduction, the Sikka archive is the only subjectively analyzed track dataset for South Asia that contains both lows and depressions, and it was compiled by manually identifying minima in maps of MSLP from the IMD and then classifying those minima by intensity. The second dataset we use is the total number of depressions forming between June and September from 1891-2019, as recorded by the IMD (`http://www.rmcchennaieatlas.tn.nic.in`). We also use IMD best track data for depressions for 1982-2018.

2.2 Reanalyses

Five global atmospheric reanalyses are used for this study, with horizontal grid spacings ranging from 0.25-1.25° and temporal resolutions ranging from hourly to 6-hourly (Table 1). The variables used are MSLP, surface wind and surface height, and the 850 hPa horizontal wind and relative humidity. All of the reanalyses used here assimilated both satellite and conventional (e.g. surface station and radiosonde) observations that increased in number and type over time, with the greatest growth seen in satellite observations. For example, ERA-Interim, produced by the European Centre for Medium-Range Weather Forecasts (ECMWF), assimilated more than 10^6 daily observations in 1989 and almost 10^7 per day in 2010; the great majority of these, by count, are from satellite, but surface and radiosonde observations from land and ship–based stations are also included, with a reasonable count over South Asia (Dee et al., 2011).

The most recent reanalysis from ECMWF, ERA5, incorporates newly reprocessed observations and input from more recent instruments that were not assimilated into ERA-Interim (Hersbach & Dee, 2016; Hersbach et al., 2019). Similarly, the Modern–Era Retrospective Analysis for Research and Applications, version 2 (MERRA-2) (Gelaro et al., 2017) and the Climate Forecast System Reanalysis (CFSR) (Saha et al., 2010) both assimilate observations not included by their predecessors, with large increases in observation counts in recent decades. In MERRA-2, for example, the

number of assimilated aircraft observations increased gradually by a factor of about four from the late 1990s to 2015, eventually becoming the dominant source of direct measurements of upper-level winds, while large step-like increases in the number of assimilated satellite radiances occurred in 2002, 2008, and 2013 (McCarty et al., 2016). Since we are interested in the large changes in monsoon depression counts seen in IMD data in the late 1970s and early 1980s, we also use the Japanese 55-year Reanalysis (JRA-55) (Ebita et al., 2011; Kobayashi et al., 2015) which extends back to 1958. Only conventional observations were assimilated by JRA-55 before 1971, and the greatest increase in the number of assimilated satellite observations occurred after 1979.

Some of the reanalyses we use include time-varying climate forcings that may influence trends in LPS activity. For example, ERA5 incorporates the Coupled Model Intercomparison Project 5 (CMIP5) radiative forcing, accounting in a self-consistent manner for changing greenhouse gases, volcanic eruptions, sea surface temperarture (SST), and sea-ice cover (Hersbach & Dee, 2016; Hersbach et al., 2019). This contrasts with ERA-Interim, which imposes a simple linear trend in greenhouse gas concentrations and uses a succession of different SST and sea ice datasets with some temporal discontinuities (Dee et al., 2011). CFSR incorporates time-evolving greenhouse gases, aerosols, and solar variations, while JRA-55 includes time-varying greenhouse gases but a two-dimensional monthly climatology of aerosol optical depth. MERRA-2 uses a sophisticated assimilation of aerosol observations, together with prescribed increases in carbon dioxide.

2.3 Precipitation and SST data

We employ several additional datasets to create indices used in assessing interannual variations of LPS activity. Indian summer rainfall is obtained from the Indian Institute of Tropical Meteorology (IITM; `http://www.tropmet.res.in/Data\`
`%20Archival-51-Page`) and is used to identify pluvial and drought summer monsoon years. The Oceanic Niño Index (ONI) is used as an ENSO indicator, and obtained from the Climate Prediction Center (`https://origin.cpc.ncep.noaa.gov/`
`products/analysis_monitoring/ensostuff/ONI_v5.php`). Monthly mean SST from the Hadley Centre Global Sea Ice and Sea Surface Temperature version 2 dataset (HadISST2)(Rayner et al., 2003) is used to compute the Indian Ocean Dipole (IOD) index; specifically, we use a normalized index represented by the anomalous SST difference between the western (10°S–10°N, 50°–70°E) and eastern (10°S–Equator, 90°–110°E) Indian Ocean.

Table 1. Details of reanalysis data used in this study.

Dataset	Spatial resolution	Temporal resolution	Period	Source
Era-Interim	$0.75° \times 0.75°$	6 hour	1979-2018	Dee et al. (2011)
JRA-55	$1.25° \times 1.25°$	6 hour	1958-2019	Ebita et al. (2011)
CFSR	$0.5° \times 0.5°$	6 hour	1979-2010	Saha et al. (2010)
MERRA-2	$0.625° \times 0.5°$	3 hour	1980-2019	Gelaro et al. (2017)
ERA5	$0.25° \times 0.25°$	1 hour	1979-2019	Hersbach et al. (2019)

2.4 TempestExtremes

An automated Lagrangian pointwise feature tracker, TempestExtremes, is used for extracting LPS track information from the reanalyses (Ullrich & Zarzycki, 2017). TempestExtremes has been used for tracking features including tropical cyclones, ex-

tratropical cyclones, and tropical easterly waves (Ullrich & Zarzycki, 2017; Chavas et al., 2017; Zarzycki et al., 2017; Michaelis & Lackmann, 2019). The basic algorithm uses the MapReduce technique, which operates in two stages: first, parallel identification of suitable candidates at each time step through application of thresholds and/or criteria that enforce a closed contour around the candidate points; second, stitching of nearby candidates over successive time steps to develop object tracks, eliminating candidates that do not exhibit behavior consistent with a transiting feature. Here, we use the specific requirement that candidate points must be within 3 degrees of each other on successive time points to be linked. If no points exist within 3 degrees of an existing point in the succeeding 12 hour period, then the track is terminated. The criteria for initial identification of suitable candidates explored in this work require identifying features that are local minima or maxima, tagging only the strongest candidate within 5 degrees great-circle distance, and testing for a closed contour in a specified search variable of specified magnitude and within a specified distance. The closed contour criterion is assessed via a depth-first search of grid points away from the nodal feature, ensuring that all possible paths away from the feature reaching the prescribed distance exhibit an increase (or decrease) in the search variable of sufficient magnitude. One minor additional modification is made to remove LPS that may appear due to artifacts of the representation of high orography in reanalyses: we require the maximum surface geopotential within $2°$ of the LPS center to be less than 8000 m^2s^{-2} for at least 24 cumulative hours of the LPS track. That is, LPS that spend nearly their entire lifetime over elevated terrain are are not included in our dataset.

Features identified using the above procedure are initially classified as LPS. Monsoon depressions, which are strong LPS, are subsequently classified by requiring a closed contour magnitude of MSLP that is greater than or equal to 4 hPa and a maximum surface wind speed within $3°$ great-circle distance higher than 8.5 m s^{-1} sustained for at least six hours along the track, similar to the IMD classification of depressions. LPS that do not satisfy these criteria are categorized as lows.

An LPS tracked using four different search variables is shown in Figure 1. The feature is tracked successfully for all four variables in both ERA-Interim and JRA-55, despite differences in spatial resolution between these datasets. There are differences in the track length compared to the Sikka archive. Visually, tracking performed with streamfunction, geopotential, and MSLP matches the Sikka track well, whereas tracking performed using vorticity does not, producing a disjointed track in both reanalyses. We systematically evaluate the performance of different tracking variables in Section 3.

2.5 Skill metric

To assess the agreement between LPS tracks obtained from our training datasets (the reanalyses) and the reference dataset (the Sikka archive), an event-matching algorithm is employed. Tracks are considered matched between two or more datasets when their points lie within $3°$ great-circle distance of each other for at least one day in their lifetime. The degree of match between tracks in the training and reference datasets is first quantified in terms of a hit ratio and false alarm ratio . The hit ratio is the fraction of matches in the reference dataset also detected in a training dataset. The false alarm ratio is the fraction of features in a training dataset without a match in the reference dataset.

We also use the Critical Success Index (CSI) (Di Luca et al., 2015) to assess algorithm skill. This index accounts for both matches and non-matches using a single skill score,

$$\text{CSI}(\text{dataset}, \text{reference}) = \frac{\langle \text{matches} \rangle}{\langle \text{matches} \rangle + \langle \text{non-matches} \rangle}. \tag{1}$$
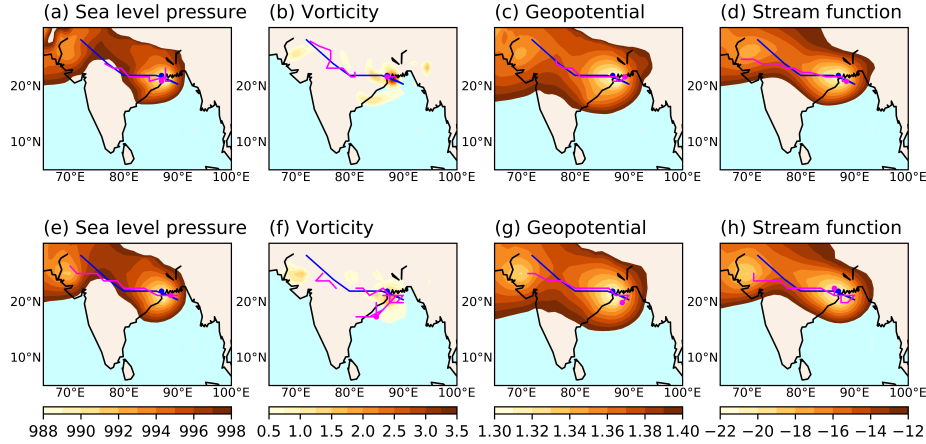
Figure 1. An illustration of LPS tracking using different search variables. The shaded region is (a, e) mean sea level pressure in hPa, (b, f) vorticity at 850 hPa in 10^{-4} s^{-1}, (c, g) geopotential at 850 hPa in 10^4 m^{2}s^{-2} and (d, h) streamfunction at 850 hPa in 10^6 m^{2}s^{-1} on 26–July–2003 00:00 UTC, corresponding to the point of maximum strength during the lifetime of an LPS. The LPS genesis point and track obtained using the given search variable are shown as the magenta dot and line, respectively. The blue dot and line are the Sikka archive LPS genesis point and track, respectively. The top panel shows results from ERA–Interim and the bottom panel from JRA-55.

Here ⟨matches⟩ is the count of matches between a training dataset and the reference dataset, and ⟨non-matches⟩ is the average count of non-matches in the training and reference datasets.

Since the reference dataset (the Sikka archive) may contain errors, it is inadequate to simply choose a tracking algorithm that maximizes the CSI for this single reference dataset. Hence, we also consider the degree to which a track is represented similarly across all reanalyses. We create a combined CSI that weights agreement between all of the reanalyses with agreement between the reanalyses and the Sikka archive,

$$\text{CSI}_{combined} = \frac{\text{CSI}_{EJCM} + \frac{\text{CSI}_{ES} + \text{CSI}_{JS} + \text{CSI}_{CS} + \text{CSI}_{MS}}{4}}{2}. \tag{2}$$

Here CSI_{EJCM} is the CSI among all four reanalyses—namely, considering ⟨matches⟩ to be the count of LPS common in all four reanalyses and ⟨non-matches⟩ to be the average of non-matches among all four reanalyses. In the latter case, we define a non-match as occurring in a particular reanalysis when the LPS detected in that reanalysis is not identified in at least one other reanalysis. The terms CSI_{ES}, CSI_{JS}, CSI_{CS} and CSI_{MS} are the four CSI values of the four individual reanalyses (ERA-Interim, JRA-55, CFSR, and MERRA-2, respectively) compared with the Sikka archive. The combined CSI is employed to rank the performance of each tracking algorithm.

3 An optimized tracking algorithm

Since monsoon lows and depressions have weaker intensities than classic tropical cyclones, it has been a challenge to detect and classify these LPS in reanalyses. A variety of methods have been used for this task, with relatively low levels of agreement between the resulting track datasets. For example, Hurley and Boos (2015) and Hunt

et al. (2016) both identified LPS as cyclonic extrema of lower tropospheric relative vorticity having concurrent negative anomalies of MSLP relative to a 21-day mean. Those studies used only ERA-Interim data. Praveen et al. (2015) identified LPS in both ERA-Interim and MERRA with a detection algorithm designed to mimic the manual identification of LPS performed by IMD, thus using only MSLP. Even when mimicking the traditional detection methodology, Praveen et al. (2015) obtained only modest correspondence with the Sikka archive: correlation coefficients for interannual variations of monsoon LPS counts were 0.4 and 0.5 for ERA-Interim and MERRA, respectively, referenced to the Sikka archive. All of the above studies chose thresholds (e.g. a 2 hPa MSLP anomaly) for their detection algorithms based on some combination of physical understanding and traditional identification methods, with little systematic assessment of those thresholds.

3.1 Candidate variables and thresholds

Here we assess multiple candidate variables and detection thresholds to obtain a tracking algorithm that is more nearly optimal across multiple reanalyses. Although it is possible that every reanalysis and every particular configuration of an atmospheric model will have a unique geophysical variable and set of thresholds that allow LPS identification to best match traditional methods (e.g. those used by IMD), retuning tracking algorithms in this way is undesirable from the perspectives of both practicality and scientific understanding. So we perform a sensitivity analysis using a set of candidate variables, with ranges of corresponding thresholds and the skill metric defined above (the CSI).

We include MSLP and the 850 hPa relative vorticity (ζ) in this set of candidate variables because these have previously been used for tracking monsoon LPS and, more generally, tropical cyclones (for a relevant history see Bengtsson et al. (1982), Broccoli and Manabe (1990), and Appendix B of Ullrich and Zarzycki (2017)) Drawbacks exist for both of those variables, with peak values of vorticity depending on the horizontal resolution of the underlying dataset, and MSLP being only an indirect indicator of the circulation several kilometers above the surface, where monsoon LPS typically have strongest winds. For this reason, we also consider the 850 hPa geopotential, which provides the geostrophic circulation closer to the level of strongest winds. Additionally, we consider the streamfunction (ψ) of the horizontal wind; through the relation $\nabla^2\psi = \zeta$, it has an exact relation to the relative vorticity but is much smoother than that variable. The geopotential and MSLP are similarly related to the vorticity only under conditions of low Rossby number, and monsoon depressions can easily achieve Rossby numbers of 2 (Boos et al., 2015). A practical challenge exists when computing ψ on a level of a vertical coordinate system that intersects the ground, because boundary conditions must be imposed on that intersection when inverting the winds (or vorticity) to obtain the streamfunction. Some reanalyses (e.g. ERA-Interim) extrapolate winds beneath Earth's surface, and we choose to replace those extrapolated values with zero prior to inverting ζ to obtain ψ. More discussion of issues involved in calculating the streamfunction is provided in Appendix A. In summary, the set of variables used to create candidate tracking algorithms are MSLP, 850 hPa relative vorticity, 850 hPa geopotential, and 850 hPa streamfunction (see also Table 2). We later test the sensitivity of the chosen geophysical variable to the choice of vertical level.

Detection of LPS involves using TempestExtremes to locate minima of MSLP, geopotential, or streamfunction, or maxima of vorticity, then testing whether that extremum is surrounded by a closed contour of the same field within a specified radius. Use of the closed contour criterion reduces the sensitivity of the method to resolution and furthermore resembles traditional methods, as discussed above. See Ullrich and Zarzycki (2017) for details on how TempestExtremes implements the closed contour criterion. We test eight closed contour magnitudes and two radii for identifying ex-

trema, with the closed contour magnitudes and radius together essentially specifying a minimum radial gradient that must exist for the extremum to be classified as an LPS. We use radii of 5° and 10° of great circle distance, with the eight closed contour magnitudes for each candidate variable shown in Table 2. This approach is analogous that used by Zarzycki and Ullrich (2017) in developing optimal criteria for identification of tropical cyclones using TempestExtremes.

Table 2. Variables and closed contour magnitudes used for detecting low pressure systems.

Search variable	Closed contour magnitudes
Mean sea level pressure (Pa)	25, 50, 75, 100, 125, 150, 175, 200
Geopotential at 850 hPa (m^2s^{-2})	25, 50, 75, 100, 125, 150, 175, 200
Streamfunction at 850 hPa (10^5 m^2s^{-1})	5.0, 7.5, 10.0, 12.5, 15.0, 17.5, 20.0, 25.0
Relative Vorticity at 850 hPa (10^{-5} s^{-1})	2.5, 3.0, 3.5, 4.0, 4.5, 5.0, 5.5, 6.0

We additionally desire a criterion for distinguishing LPS from "heat lows", which are non-precipitating low pressure systems trapped in the lower troposphere (Ramage, 1971; Rácz & Smith, 1999). Heat lows frequently form over northwestern India during summer and over central India before monsoon onset there; they fulfill all the traditional kinematic criteria for LPS discussed in the Introduction, but seem to be traditionally excluded from LPS datasets by some implicit criteria that we suspect involves their geographic location or moisture content. We initially attempted to use a precipitable water criterion to distinguish heat lows from traditional LPS, but recognized that the increase in precipitable water expected in a warming climate might create spurious trends in LPS counts. One alternative would be to require a minimum precipitation rate to distinguish heat lows from LPS, motivated by the fact that most interest in LPS exists because of their heavy precipitation. But precipitation rates have large variance on short time and space scales, and are also subject to trends in a warming climate. So we opt to distinguish LPS from heat lows using the 850 hPa relative humidity (RH), averaged within 3° of the LPS center. Eight RH thresholds ranging from 55% to 90%, with an interval of 5%, are used in the candidate tracking algorithms. The RH is required to exceed these thresholds for a cumulative period of at least one day over the disturbance lifetime to be considered an LPS, otherwise it is categorized as a heat low. This choice thus includes systems in our LPS dataset that spend much of their lifetimes as non-precipitating, low-RH disturbances but that achieve high lower-tropospheric RH for at least one day.

3.2 Assessing candidate tracking schemes

Using the above sets of candidate variables, closed contour magnitudes, radii, and RH criteria, we use TempestExtremes to identify LPS in four reanalyses (ERA-Interim, JRA-55, CFSR, and MERRA-2; see Table 1) for the training period of 1990–2003. This 14-year training period is chosen to overlap with the Sikka archive, which ends in 2003, while leaving a substantial period for verification (1979-1989). A total of 2,048 track datasets are thus created (4 reanalyses × 4 candidate variables × 8 closed contour magnitudes × 2 radii × 8 RH thresholds). The maximum surface wind speed within 3° of the center is used as the maximum sustained surface wind speed of a storm at a time step, and is used later to classify disturbances as lows and depressions. The land-sea ratio of the grid point at the center of each LPS is used for region-wise categorization, with storms treated as being over land when this ratio is higher than 0.5. The TempestExtremes commands for tracking LPS using these criteria is provided in Appendix B.

We perform a sensitivity analysis by ranking the 512 tracking algorithms, for each of the four reanalyses, by the combined CSI (Figure 2). As described in the previous section, the combined CSI is a weighted average of the agreement of each reanalysis track dataset with the Sikka archive and the agreement between all reanalyses. The top 31 algorithms by this ranking all use the 850 hPa streamfunction. The top-ranked algorithm requires a disturbance to have an 850 hPa streamfunction that increases by 1.25×10^6 from the center minimum within a radius of $10°$, while achieving an 850 hPa RH of at least 85% for at least one day. The second-best variable for tracking LPS is the 850 hPa geopotential (closed contour magnitude of 125 m² s⁻² and RH higher than 85%). The lower ranking (32 out of 512) of the geopotential comes mainly from greater disagreement between reanalysis tracks, i.e. a smaller value of CSI_{EJCM} in Equation 2, and algorithms based on geopotential are only slightly less skillful than those based on streamfunction (Figure 2). Since streamfunction is not included in most reanalyses and must be computed prior to running the tracking algorithm, the geopotential is a viable alternative for LPS tracking that requires only a slight compromise in skill. Algorithms based on MSLP have lower skill, with the highest rank of 133 (out of 512); the lower rank comes mainly from greater disagreement between reanalyses but with some contribution from disagreement with the Sikka archive (not shown). The least skillful algorithms all use the 850 hPa vorticity, with the highest rank of 359 out of 512. The vorticity-based algorithms produce track datasets that disagree most strongly between reanalyses and that differ most with the Sikka archive. This is notable given the number of past studies that have used vorticity or potential vorticity to track synoptic-scale monsoon disturbances in Asia, Africa, and Australia (Hurley & Boos, 2015; Hunt et al., 2016; Thorncroft & Hodges, 2001; Berry et al., 2012). Variables and thresholds for the top-five ranked algorithm and top algorithm of each searching variable are depicted in Table S1.
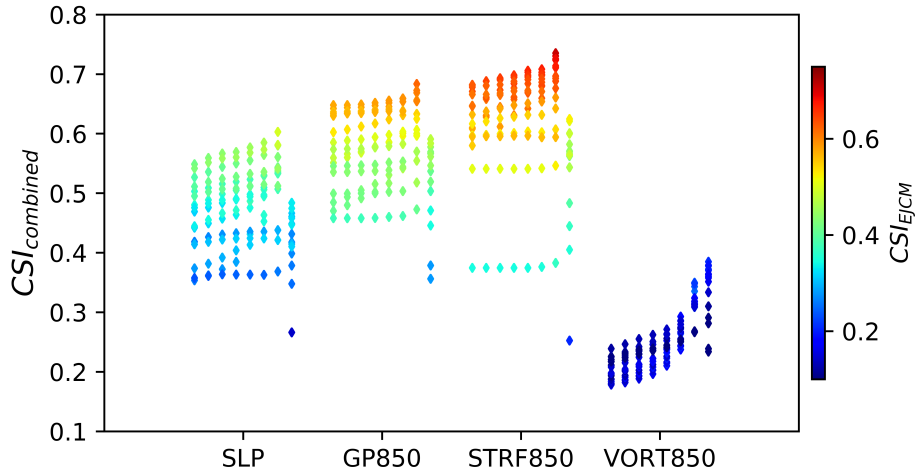

Figure 2. Illustration of the greater skill of 850 hPa streamfunction in detecting LPS. Each diamond marks the combined Critical Success Index (defined in text) for one combination of closed contour magnitude, radius, and RH threshold. Shading represents consistency of the algorithm across reanalyses. The tested variables were mean sea level pressure (SLP), 850 hPa geopotential (GP850), streamfunction of the 850 hPa horizontal wind (STRF850), and 850 hPa relative vorticity (VORT850). Each column within a variable represents one RH threshold, from 55% (left) to 90% (right) with an interval of 5%.
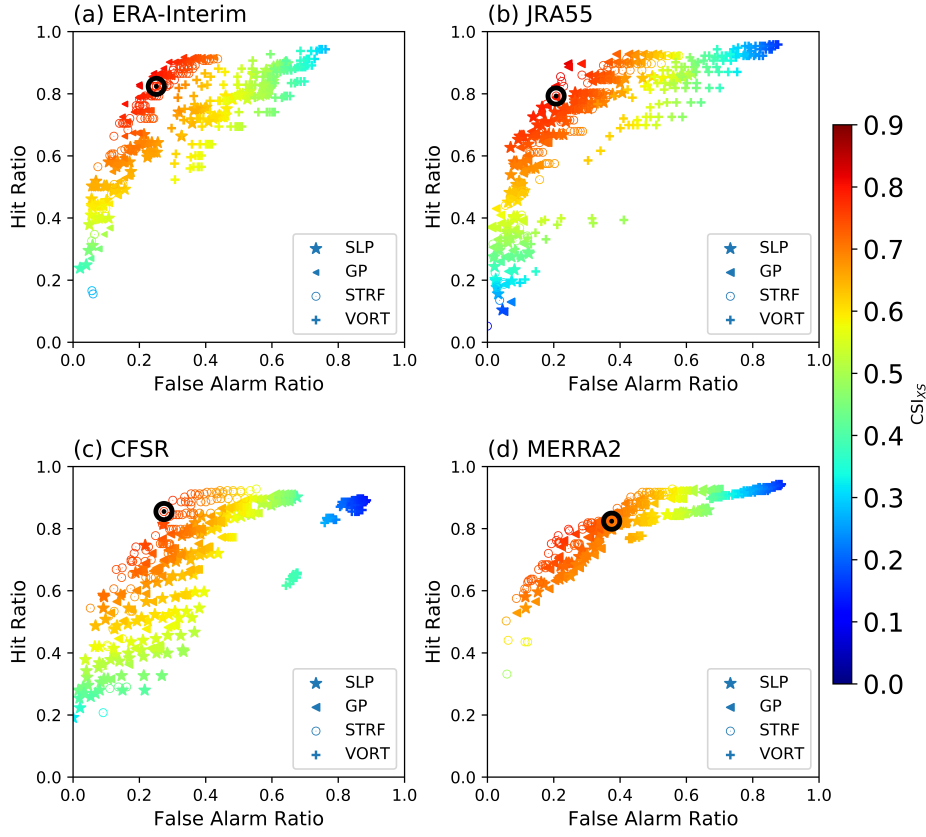
Figure 3. Hit ratio vs. false alarm ratio (see text for definition) with respect to the Sikka archive for all LPS algorithms, shaded by CSI_{XS} for: (a) ERA-Interim, (b) JRA-55, (c) CFSR, and (d) MERRA-2. The black circle represents the selected optimal algorithm (top-ranked by the combined CSI).

Although the consistency of an algorithm across reanalyses constitutes a large part of its skill score, the top-ranking algorithm also captures more than 80% of LPS in the Sikka archive, our reference dataset. The fraction of LPS in the Sikka archive that are detected in reanalyses (the hit ratio) is plotted against the fraction of LPS detected in reanalyses that do not exist in the Sikka archive (the false alarm ratio) in Figure 3. Tracking algorithms using the 850 hPa streamfunction and 850 hPa geopotential have higher CSI values with higher hit ratios and lower false alarm ratios in all reanalyses. In most reanalyses, algorithms based on MSLP have smaller hit ratios than those based on streamfunction or geopotential. Vorticity-based algorithms have lower CSI values mainly due to higher false alarm ratios in all reanalyses. The top-ranked algorithm by the combined CSI (marked by black circles in Figure 3) compares well with the Sikka dataset in all reanalyses, with hit ratios of about 0.8 and false alarm ratios around 0.3.

We also compute the skill scores outside the training period (in the validation period of 1979–1989), finding that there is little change in the level of agreement between each reanalysis and the Sikka archive; the CSI of ERA-Interim, JRA-55, CFSR and MERRA-2 are 0.79, 0.80, 0.79 and 0.71, respectively, in the training period

and 0.78, 0.78, 0.77 and 0.72, respectively, in the validation period. Remarkably, ERA5, which was not used for training, has a higher CSI (0.83), a higher hit ratio, and a lower false alarm ratio than the other reanalyses. This is true despite the fact that ERA5 has hourly, 0.27° resolution while the reanalyses used for algorithm training have grid spacings coarser by factors of 2-6.

For completeness, we also checked whether combining MSLP and 850 hPa vorticity might improve the tracking algorithm, since previous studies used such combinations of variables (Hurley & Boos, 2015; Hunt et al., 2016). Algorithms using a combination of MSLP and vorticity had CSI values around 0.6, similar to those based on MSLP alone. Furthermore, combining streamfunction and vorticity did not noticeably improve the skill scores. Finally, we tested whether the skill score would improve by using a variable from a different vertical level. Using the streamfunction of horizontal wind at 1000 hPa, 700 hPa, and 500 hPa yielded CSI values lower than those obtained for the 850 hPa streamfunction.

Using the top-ranked algorithm, we track LPS in all available years of all reanalyses (Table 1). This includes ERA5, which was not used for training.

3.3 Are non-matches real systems?

We now check whether the "false alarms"—LPS identified in reanalyses by our top-ranking algorithm but missing in the Sikka archive—exist due to some error or artifact in the tracking algorithm. We do this by comparing composites of the structures of reanalysis LPS that match those in the Sikka archive with composites of those missing from the Sikka archive. We do this separately for monsoon lows and monsoon depressions, since the implications of a false alarm are different when the LPS is a weak LPS compared to a strong one. We furthermore only include a reanalysis LPS in our composites of false alarms when it is completely missing from the Sikka archive, as opposed to when it is categorized differently (e.g. here we ignore LPS that are classified as a depression in a reanalysis but a low in the Sikka archive). These composites are made using ERA5, since that reanalysis was not used in tuning the tracking algorithm. There are 57 lows and 10 depressions in ERA5 that are missing from the Sikka archive. Composites are created by averaging, in a storm-centered reference frame, the three time steps having the largest central MSLP anomaly.

The composites of lows and depressions have structures consistent with those seen in prior studies (Godbole, 1977; Hurley & Boos, 2015), and these exhibit relatively little differences between matches and non-matches (Figure 4). The LPS all consist of a column of cyclonic potential vorticity (PV) that extends from the surface to the upper troposphere, with primary maxima near 500 hPa and secondary peaks around 850 hPa. The composite relative vorticity is more bottom-heavy, peaking near 800 hPa. Both the PV and relative vorticity tilt slightly westward with height and are stronger in depressions than in lows, as expected. For lows, the non-matches (i.e. those present in ERA5 but missing from the Sikka archive) are weaker than the matches, perhaps because the 850 hPa streamfunction in ERA5 represents weaker systems than were contained in the MSLP maps on which the Sikka archive was based, or perhaps because our tracking algorithm was better able to detect weak systems than the subjective analysis used by the Sikka archive. There is no clear difference between the composites of matching and non-matching depressions, with any quantitative differences in magnitude likely not significant considering the low number (10) of non-matches. Comparisons of composites of winds, relative humidities, and temperatures yielded similar results (not shown).

We furthermore obtained the daily MSLP charts from the IMD, which are thought to be similar to those on which the Sikka archive was based, and manually inspected these to search for the ten depressions present in ERA5 but missing in the Sikka
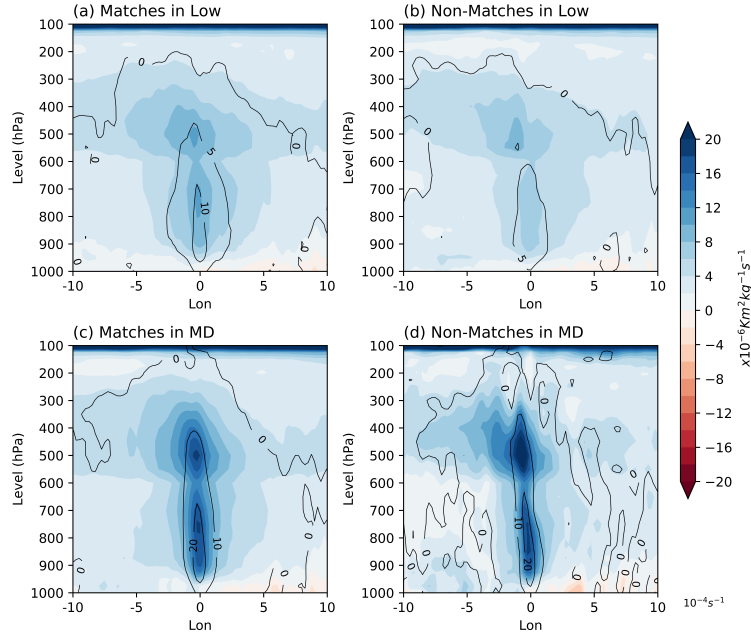
Figure 4. Composite of the vertical cross-section of potential vorticity (shaded) and relative vorticity (contours), through the central longitude of the system, for (a) matches in lows, (b) non-matches in lows, (c) matches in depressions and (d) non-matches in depressions.

archive. At the times and locations of all ten of these missing depressions, we found LPS-like features in the pressure charts, with three of the charts clearly showing disturbances marked on the charts as depressions or a more intense category of LPS. We conclude that the ten additional depressions in ERA5 are real and were somehow missed when the Sikka archive was created.

4 Assessing the LPS climatology in reanalyses

We now examine the climatological mean distributions of genesis density, track density, disturbance lifetime, and track length, with the goal of assessing whether the overall statistics of disturbances identified in reanalyses agree with the well-known statistics of monsoon LPS.

4.1 Genesis

The boreal summer (June-September) distributions of genesis frequency for all LPS are broadly similar among all reanalyses and the Sikka archive (Figure 5). The latter has genesis more concentrated over the northern Bay of Bengal, but with a total number of LPS—14 per summer—similar to that in most of the reanalyses. The total count is higher in MERRA-2 and CFSR, around 18 per summer.

There is general agreement amongst the reanalyses, and between the reanalyses and the Sikka archive, regarding the partitioning of LPS into lows and depressions, the rate of genesis over land compared to that over ocean, and the seasonal cycle of
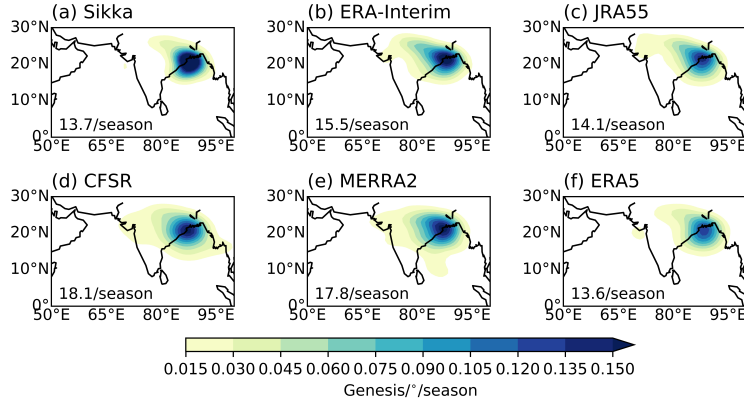
Figure 5. Genesis density of LPS for the period of 1980–2003 in the Sikka archive and re-analyses. Kernel density estimates are used to calculate the genesis density. Numbers in the bottom-left corner represent the mean number of LPS in a season for the period.

genesis (Figure 6). The most notable outlier is MERRA-2 which, unlike the other four reanalyses and the Sikka archive, has more depressions than lows.

Consistent with the spatial distributions of genesis shown in Figure 5, most reanalyses also represent a larger fraction of LPS forming over land, compared to the Sikka archive (Figure 6). ERA5 has the fewest LPS of all the reanalyses, though the difference is relatively small, and the ERA5 total count is an almost exact match to the Sikka archive. The match with the Sikka archive is notable because ERA5 was not included in the algorithm's training dataset. All the reanalyses also capture the greater frequency of LPS in the middle of summer, although ERA5 shows slightly greater frequency in July while all other reanalyses and the Sikka archive show greatest frequency in August. This seems to be an improvement over previous reanalysis-based tracking algorithms, which showed genesis occuring more frequently in June than in August in ERA-Interim (Hurley & Boos, 2015).

4.2 Track density and lifetime of LPS

All the reanalyses show a similar track density distribution to that seen in the Sikka archive, although the reanalyses extend further westward toward northwestern India (Figure 7). The highest track density over land is found in MERRA-2; that reanalysis also has the highest number of days with an LPS present, which is due to both the high genesis frequency and high LPS lifetime in MERRA-2 (Figure 8).

Lifetimes are generally longer in the reanalyses, with the longest found in ERA5, which has LPS lasting one to two days longer than the Sikka archive. The distributions of lifetimes for all LPS are more strongly skewed in the reanalyses than in the Sikka archive, with the median lifetime being almost a full day longer than the mean lifetime (Figure 8a). Track lengths (in great circle distance between start and end points) are similar between the reanalyses and Sikka archive, implying a slower translation speed in the reanalyses: 2.3 m s^{-1} in the Sikka archive and 1.6 m s^{-1} - 1.91 m s^{-1} in the reanalyses. In all datasets, depressions have longer tracks and lifetimes than lows, and tracks and lifetimes are longer over ocean than over land.
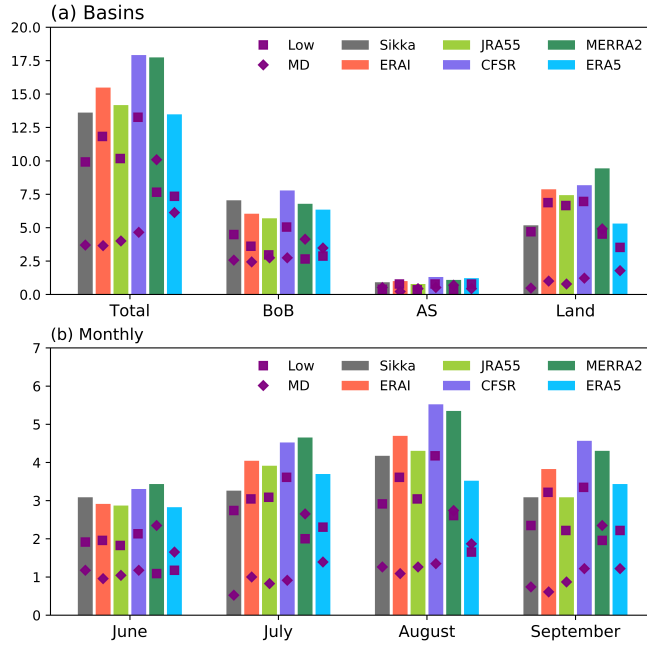
–14–

Figure 6. (a) The summer monsoon season (JJAS) climatology, for the Sikka archive and reanalyses, of the number LPS formed over the north Indian Ocean basin and subregions of the Bay of Bengal (BoB), Arabian Sea (AS), and Indian land mass (Land). (b) Climatological monthly variation of LPS. monsoon lows and monsoon depressions are represented as squares and diamonds respectively. The period of analysis is 1980–2003.
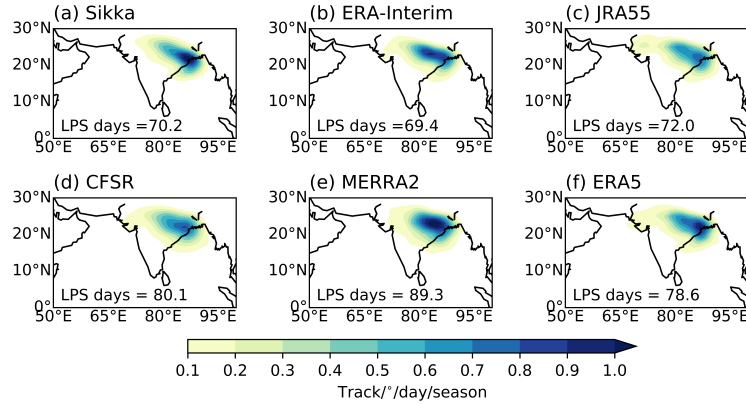

Figure 7. Track density of LPS for the period of 1980-2003 in the Sikka and reanalyses. Kernel density estimates are used to calculate the track density of LPS. Numbers in the bottom-left corner represent the mean number of days in which LPS are present in a season for the period.

5 Interannual and long term variations

5.1 Interannual correlations between datasets

The interannual variability of seasonal total counts of LPS, lows, and depressions has a similar magnitude across reanalyses and the Sikka archive, but these variations
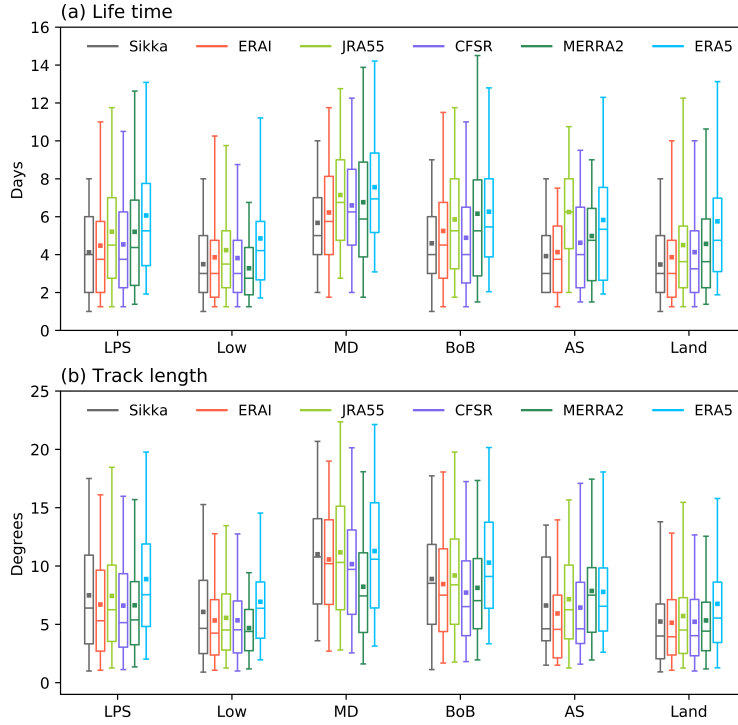
Figure 8. Box-and-whisker plots of (a) lifetime (b) track length of LPS in Sikka archive and all reanalyses. The horizontal line within the boxes indicates the median, boundaries of the boxes indicate the 25th and 75th percentile, the whiskers indicate the 5th and 95th percentile values, and the solid square represents the mean value. The period of analysis is 1980–2003.

exhibit low to modest correlation between data products (Figure 9a). The correlations between different reanalyses of seasonal LPS counts range from about 0.5 to 0.75, higher than the 95% confidence level of 0.34 for this sample size, with the two ECMWF reanalyses being most strongly correlated. The dataset having the weakest correlations with all others is the Sikka archive; the LPS dataset of Hurley and Boos (2015) also showed little interannual correlation with the Sikka archive. This might arise due to differences in the geophysical observations on which each dataset is based, on the variables used for tracking, and on other methodological details. In particular, LPS in the Sikka archive were identified through manual analysis of surface pressure charts, which were in turn obtained through manual analysis of station observations; such subjective methods might introduce random and/or systematic errors (e.g., a bias toward identifying LPS over land).

Some brief statistical modeling illustrates the effect of such errors on interannual correlations. We state in Section 3.3 that 67 LPS are present in ERA5 but not in the Sikka archive; these non-matching storms reduce the interannual correlation between those two datasets. We test the sensitivity of the interannual correlations to missing storms by removing random LPS from the Sikka archive between 1979 and 2003, adding the same number of "false alarm" LPS to random years in that archive, then recalculating the interannual correlation with the original Sikka archive. Removing 67 random storms (20% of the archive) and adding the same number of false alarms

degrades the correlation coefficient from 1.0 to an average of 0.62 (with a 95% confidence interval of 0.36-0.81, empirically sampled from 1,000 iterations). Increasing the fraction of randomly replaced storms to 30% of those in the Sikka archive further degrades the correlation coefficients, in this statistical model, to the range of 0.1-0.2 seen for correlations between the Sikka archive and most reanalyses. Thus, the relatively low interannual correlation each reanalysis has with our reference dataset is consistent with the hit ratios and false alarm ratios seen in Figure 3. We note that the interannual correlation between the Sikka archive and ERA–Interim (0.53) is higher than reported by Praveen et al. (2015) (0.2 to 0.4); those authors detected LPS using surface pressure, which we show in Section 3.2 produces worse skill than detectors based on streamfunction (which was used in the tracking algorithm examined here).

Interannual correlations between datasets are weaker for the individual categories of lows and depressions (Figures 9b, c). These lower correlation values are likely related to differences in the categorization of lows and depressions in the Sikka archive and reanalyses. Even though the reanalyses capture more than 80% of LPS in the Sikka archive, one in three depressions in the Sikka archive are categorized as a low in the reanalyses and vice-versa. Yet there is clearly some agreement: all datasets, including the Sikka archive, capture the high number of depressions in 2006 (Figure 9d), which coincides with an Indian Ocean Dipole event (Krishnan et al., 2011).
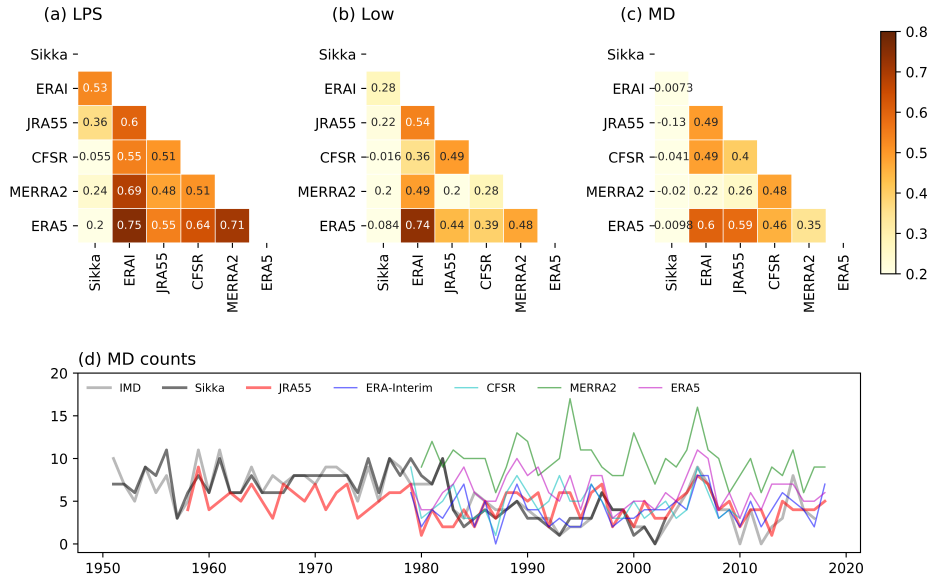

Figure 9. Interannual correlation of the number of Indian summer (JJAS) (a) monsoon low-pressure systems (b) lows and (c) monsoon depressions between the datasets includes Sikka archive and the reanalyses during 1980-2003, the years in which all LPS dataset available. (d) Year to year varaition in the number of monsoon depression in all renalysis datasets, Sikka archive and from IMD.

5.2 Relation to interannual climate modes

Given the large contribution of LPS to India's total summer rainfall (Yoon & Chen, 2005), some studies have explored whether interannual variations in LPS activ-

ity are associated with interannual variations in total Indian summer rainfall (Sikka, 2006; Krishnamurthy & Ajayamohan, 2010). We build on this by analyzing how LPS count, mean lifetime, and track length vary between pluvial and drought years in the Sikka archive and reanalyses. We define "pluvial" years as years when seasonal total rainfall is more than one standard deviation above the mean, and "drought" years as those when rainfall is more than one standard deviation below the mean. LPS counts are significantly higher in pluvial than drought years in four out of five reanalyses (Figure 10a), but there are no significant changes in lifetime and track length in four of five reanalyses (Figure S1a and S2a). Although the Sikka archive shows no change in LPS counts between pluvial and drought years between 1979 and 2003, Krishnamurthy and Ajayamohan (2010) performed the same analysis of the Sikka archive for 1901-2003 and found a higher number of LPS and a higher number of days with LPS conditions in pluvial compared to drought years. When examining how counts of the individual categories of lows and depressions change between pluvial and drought years, most reanalyses and the Sikka archive show no detectable signal (Figure 10b, c).
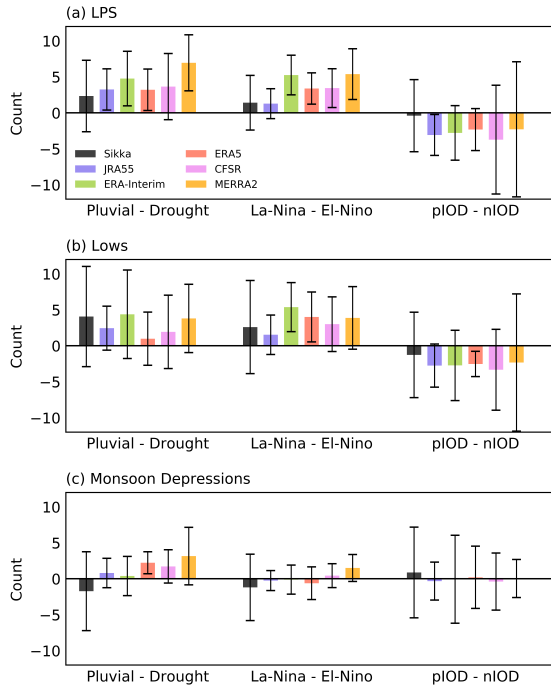

Figure 10. Difference of (a) LPS, (b) lows and (c) monsoon depression mean counts in pluvial-drought summer monsoon years, La Niña-El Niño years, and positive-negative Indian Ocean Dipole years. The vertical lines represent the 95% confidence interval for the difference in the mean counts. Analysis of each dataset set includes all available period of that datsets (see Table 1)

Interannual variation of the Indian summer monsoon is highly linked to ENSO, with an increased propensity for drought years in the warm phase of ENSO (El Niño) and pluvial years in its cold phase (La Niña). We find that LPS counts are higher in La Niña years than El Niño years (Figure 10a), and the differences are significant in all datasets except the Sikka archive and JRA-55. When assessing ENSO-related

variations in lifetimes and track lengths, the only detectable signal is in ERA-Interim and ERA5, which exhibit LPS lifetimes that are higher in El Niño years than La Niña years (contrasting with their lower average counts in those years; Figure S1a). The fact that a signal is sometimes detected in only one or two out of six datasets shows that it may be important to reexamine results from prior studies that relied on a single dataset. For example, Krishnamurthy and Ajayamohan (2010) used only the Sikka archive when showing that LPS activity is roughly equal in El Niño and La Niña years. Hunt et al. (2016) relied on only ERA-Interim when finding that depression activity is 16% higher in El Niño than La Niña years.

Finally, we examine covariations of LPS with the Indian Ocean Dipole (IOD), an SST pattern associated with variations in Indian summer monsoon circulation and rainfall (Saji et al., 1999; Webster et al., 1999). Krishnan et al. (2011) found that depressions have higher track lengths in positive IOD years, and Hunt et al. (2016) found that depression lifetime is 12% higher in positive IOD years. We find that only one reanalysis (JRA-55) shows a change in LPS counts between positive and negative IOD years, and another reanalysis (CFSR) shows longer depression lifetimes (Figure S1c and S2c). For all other datasets, the 95% confidence interval on the IOD-related changes in counts, lifetimes, and track lengths includes zero.

5.3 Trends in LPS

5.3.1 Linear trend analysis

Based on the Sikka archive and the IMD dataset of depression counts, previous studies discussed an apparent increase in the number of lows and a decrease in the number of depressions forming each summer (Jadhav & Munot, 2009; Prajeesh et al., 2013; Vishnu et al., 2016, and references therein). However, Cohen and Boos (2014) questioned the existence of a decrease in the number of depressions in the past 40 years, based on their finding that no trend in depression counts could be detected in ERA-Interim and on their discovery of depressions in that reanalysis that were missing in the IMD dataset. Here we examine whether a trend in the number of LPS overall, or in the number of lows or depressions, can be detected in any of the track datasets created using our tracking algorithm. We first assess the period since 1979, since four of our reanalyses start in that year, then compare to results starting in 1958 (for which only JRA-55, the Sikka archive, and the IMD dataset provide values).

Consistent with previous studies, the Sikka archive shows no trend in the seasonal counts of all LPS since 1979, together with an increasing trend in lows and a decreasing trend in depressions (Figure 11). Any decreasing trend in depressions in the IMD dataset is weaker and has an error bar that includes zero. None of the reanalyses show any appreciable trend in lows or depressions.

Vishnu et al. (2016) noted that the trend in depressions is not linear, but consists mainly of a large reduction around 1980, which lies at the beginning of the records discussed in the previous paragraph. Since JRA-55 is the only reanalysis with data prior to 1979, we compute the trend in depressions for the more extended period starting from 1958 in JRA-55, and compare this with trends from the IMD and Sikka datasets (Figure 11). The IMD and Sikka datasets show depression counts decreasing at a rate of -0.096 year^{-1} and -0.14 year^{-1}, respectively (with 95% confidence intervals of ± 0.032 year^{-1} and ± 0.043 year^{-1}; Figure 11, and see the time series in Figure 9d). The long-term decrease in depressions in the Sikka archive is opposed by a long-term increase in lows, resulting in no trend in total LPS. Any trend in JRA-55 is substantially smaller than in the Sikka or IMD datasets and is not significant at the 95% confidence level (Figure 11); the JRA-55 trend is -0.021 year^{-1} with a 95% confidence interval of ± 0.024 year^{-1}). No statistically significant trend is seen in the total number of LPS forming each summer in JRA-55.
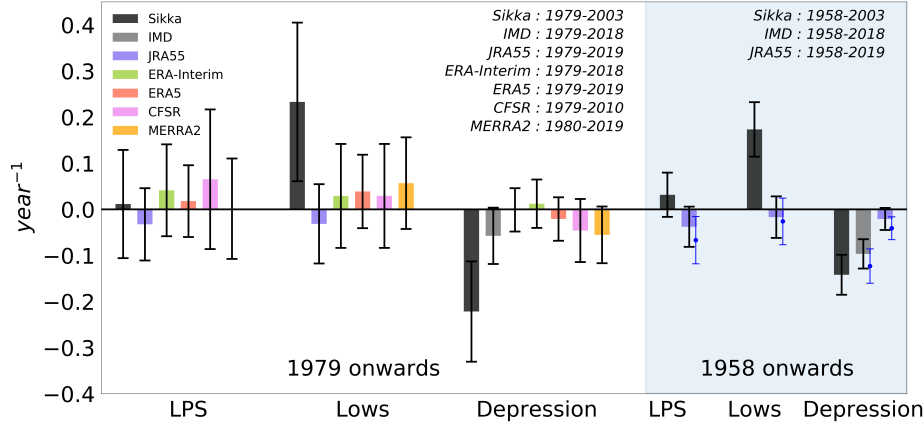
Figure 11. Linear trends in LPS, lows, and depression in the Sikka archive and reanlyses. The white shaded region shows trends from 1979 onwards, while gray shaded region shows trends for 1958 onwards. Error bars represent the 95% confidence interval for these trends. Blue dots and error bars represent the trend and 95% confidence interval, respectively, for the extended season of May to October. The 95% confidence intervals assume a normal distribution and thus are 1.96 times the standard error.

Although the Indian summer monsoon season is commonly defined as occurring June-September, with the Sikka archive available for only those months, it is possible that the results of our trend analysis would change if we used an extended season of May-October. Indeed, Xavier et al. (2007) argued that the primary effect of ENSO on Indian rainfall occurs via its influence on the duration of the rainy season, with La Niña events allowing it to extend into May and October. Including May and October in our trend analysis for the period starting in 1958 yields an increase in the magnitude of the depression count trends found in JRA-55 and the IMD dataset, with the JRA-55 trend becoming significant at the 95% confidence level (Figure 11). The total number of LPS forming in this extended summer season in JRA-55 also shows a decreasing trend that is significant at the 95% confidence level, but there is no discernible trend in lows in JRA-55. We also repeated the trend assessment, using the longer May-October season, for all reanalyses for the shorter period starting in 1979, with little change in the results: only ERA-Interim LPS show an increasing trend significant at the 95% confidence level.

We also analyze storm count trends using multiple detection algorithms, in order to explore the influence of parametric and structural uncertainty in the algorithm on our trend assessment. Specifically, we examine LPS counts obtained using the top five streamfunction-based algorithms, the top three geopotential height-based algorithms, and the top three MSLP-based algorithms. No algorithms applied to any reanalysis show a significant trend starting in 1979 (Figure S3). However, two of the nine algorithms applied to JRA-55 show a statistically significant decrease in LPS from 1958, and one of the nine shows a significant decrease in depression counts in that period. All of these trends are of similar magnitude to the those found in JRA-55 with our primary algorithm (Figure 11).
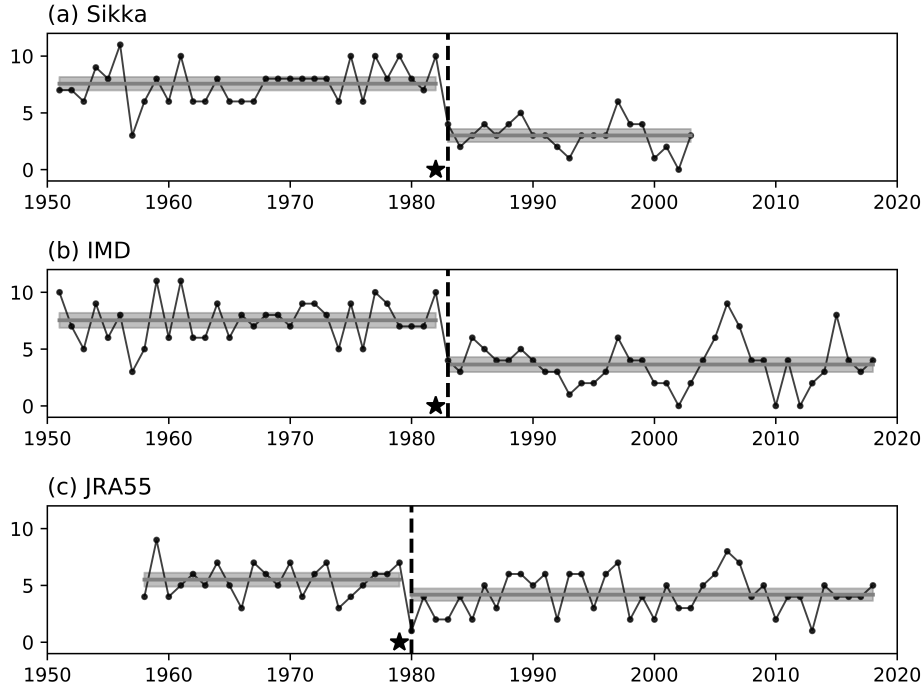
Figure 12. Illustration of a shift in depression count around 1980. Year-to-year variation of depression count (black line) in (a) Sikka archive, (b) IMD and (c) JRA-55. The vertical dash line is the mean shift in the depression count using binary change point detection. The star symbol represents the introduction of the geostationary satellites in the respective dataset. The horizontal grey line shows the annual mean value of depression count in the given epoch, and shading shows the 95% confidence interval of the mean value.

5.3.2 *Change point detection*

Like any reanalysis, JRA-55 assimilated data from an observational network that evolved over time, and we wish to consider whether this might affect any detected trends. For example, satellite data first started to be assimilated by JRA-55 around 1980, and there is a large reduction in depression counts in JRA-55 in that year (Figure 9d). We calculate the year and magnitude of a single long-term shift in the summer mean depression count using a binary change point detection method (Truong et al., 2019), and find that the mean depression count undergoes a systematic reduction in the early 1980s all datasets: 1983 in IMD and the Sikka archive and 1980 in JRA-55 (Figure 12). The shift in the mean values is larger in the IMD dataset (decreasing from 7.5 ± 0.7 year^{-1} to 3.6 ± 0.7 year^{-1}) and the Sikka archive (decreasing from 7.6 ± 0.6 year^{-1} to 3.0 ± 0.6 year^{-1}) and smallest in JRA-55 (decreasing from 5.5 ± 0.6 year^{-1} to 4.2 ± 0.5 year^{-1}). The shifts in all three data sets are statistically significant at the 95% confidence level. The shift in JRA-55 in 1980 is contemporaneous with the introduction of geostationary satellites observations to that reanalysis system in 1979 (Ebita et al., 2011), the date marked by the star in Figure 12c. Similarly, the IMD started using Indian geostationary satellite data in 1982, which is contemporaneous with the 1983 shift in depression counts in both the Sikka archive and the IMD dataset (recall that the Sikka archive was constructed by analyzing MSLP maps obtained from the IMD).

673 This suggests that the shift, and by association the linear trends discussed above, might
674 be an artifact of changes in observational data sources. Formal attribution of these
675 early-1980's shifts is beyond the scope of this manuscript, but these results suggest
676 that further study is warranted.

677 # 6 Summary and conclusions

678 Synoptic–scale monsoon LPS produce abundant rainfall over South Asia, making
679 the identification of LPS in estimates of past and future atmospheric states an impor-
680 tant task. Yet previous methods for tracking LPS have relied on subjective or auto-
681 mated methods not systematically assessed for skill or optimality (Mooley & Shukla,
682 1987; Sikka, 2006; Praveen et al., 2015; Hurley & Boos, 2015; Hunt et al., 2016). For
683 example, multiple previous LPS datasets were based entirely on MSLP, even though
684 LPS are known to have peak intensities several kilometers above the surface (Godbole,
685 1977). These issues become especially salient when examining multi-decadal trends in
686 LPS activity, because unintentional changes in a subjective method or trends in the
687 observing network on which an underlying dataset is based could bias an analyzed
688 trend.

689 This study builds on previous literature by introducing a fast and objective track-
690 ing algorithm able to identify monsoon LPS in high-resolution datasets. The method
691 is based on the feature tracking capabilities of the TempestExtremes package. A sensi-
692 tivity analysis was performed to choose an optimal algorithm using multiple reanalyses
693 of various spatial and temporal resolutions. A total of 512 algorithms (defined by dif-
694 ferent search variables and values for the closed contour criteria) are applied to four
695 reanalyses for the training period of 1990-2003. Based on a skill score, the CSI, that
696 compares the reanalyses with each other and with the Sikka archive (our reference
697 dataset), the optimal algorithm was found to use the 850 hPa streamfunction. The
698 LPS identified with this algorithm in reanalyses are found to match more than 80% of
699 LPS in the Sikka archive. The reanalyses track datasets also contain LPS not present
700 in the Sikka archive. For instance, the ERA5 dataset includes 57 lows and 10 depres-
701 sions that are entirely missing in the Sikka archive. Composites of these LPS and the
702 LPS present in the Sikka archive show similar dynamical structures, so we conclude
703 that the algorithm correctly captures LPS in the atmospheric states represented by
704 the reanalyses.

705 Characteristics of the LPS, including distributions of genesis frequency, track
706 density, intensity, lifetime, and track length, are consistent across all reanalyses and
707 are similar to results from the Sikka archive. The new reanalysis track datasets also
708 reproduce previously reported monthly and basin-wise climatological variations of LPS
709 characteristics. On interannual time scales, LPS counts in the reanalyses have weak
710 correlation with the Sikka archive. This result may be due, in part, to LPS that are
711 missing from the Sikka archive but that exist in most of the reanalyses. The better
712 correspondence between the track datasets based on five different reanalyses, with
713 horizontal resolutions ranging from 0.25° to 1.25°, gives confidence that the algorithm
714 can consistently capture LPS in datasets with different resolutions.

715 Our examination of interannual variations in LPS genesis frequency, track length,
716 and lifetimes illustrate the importance of assessing signals in multiple datasets. For
717 the period starting in 1979, we find significantly higher LPS counts in pluvial years
718 compared to drought years in four out of five reanalyses, in agreement with the longer
719 period (1901-2003) analysis of Krishnamurthy and Ajayamohan (2010). We also find
720 significantly higher LPS counts in La Niña years relative to El Niño years, again in
721 four of five reanalyses and consistent with Krishnamurthy and Ajayamohan (2010).
722 Associations between LPS counts and the Indian Ocean Dipole are detected in only
723 one reanalysis, despite the fact that Krishnan et al. (2011) and Hunt et al. (2016)

reported enhanced depression activity in positive IOD years. The higher depression activity in El Niño years reported by Hunt et al. (2016) was also not seen in any of the reanalyses we examined.

Past studies of long-term trends in the IMD and Sikka datasets have found increases in the number of lows and decreases in the number of depressions (Rajendra Kumar & Dash, 2001; Prajeesh et al., 2013; Vishnu et al., 2016). Here, however, we do not detect statistically significant trends in summer counts of lows or depressions in any reanalysis for the period from 1979 onwards (the Sikka archive has a strong decrease in depression counts and an increase in lows for that period). The JRA-55 reanalysis, which provides data starting in 1958, shows a statistically significant reduction in depression counts only when using an extended summer season (May-October), and this trend is about one-quarter the magnitude of the trend seen in the IMD dataset and Sikka archive. Furthermore, a binary change point detection analysis shows that the long-term decrease is consistent with a step-wise reduction in depression counts in the year following the introduction of geostationary satellite data into the datasets underlying the IMD, Sikka, and JRA-55 products. This suggests the possibility that no long-term reduction in depressions has occurred, and trends seen in existing data products may be artifacts of change in the observing network; further analysis is warranted.

The new and objective LPS datasets developed here have been made publicly available, together with the tracking algorithm, to allow their broad use in characterizing LPS activity and understanding LPS dynamics (doi:10.5281/zenodo.XXXXX) *[the datasets will be finalized and uploaded, and a DOI obtained, after addressing reviewer comments that may require modification of the datasets].* These datasets and the tracking algorithm may also be useful in assessing LPS activity in ensembles of global climate models and in characterizing and correcting bias in forecasts made by numerical weather prediction models. The future release of new reanalysis data for years preceding 1979, such as is expected for ERA5 (Hersbach & Dee, 2016), will also provide new opportunities to reexamine long-term trends in LPS activity, especially since those reanalyses include representations of historical climate forcings by greenhouse gas, aerosol, and land use changes.

Appendix A Boundary conditions for streamfunction inversion

A practical challenge exists when computing the streamfunction, ψ, of the horizontal wind, $\vec{u}$ on a level of a vertical coordinate system that intersects the ground: boundary conditions must be imposed on that intersection when inverting the winds (or vorticity) to obtain ψ. That is, the uniqueness of the Helmholtz decomposition that holds in a spherical domain without boundaries breaks down, and a class of harmonic functions can be added to ψ while still allowing $\nabla^2\psi$ to correctly represent the local vertical vorticity. Numerous ways of dealing with this nonuniqueness have been proposed in the context of atmospheric and oceanic flow (Lynch, 1988). One method requires the velocity potential, ϕ to vanish on the boundaries, minimizing the kinetic energy in the divergent part of the flow (Sangster, 1960; Pedersen, 1971). Another method requires ψ to be constant along a boundary (Watterson, 2001); this is appropriate when there is zero horizontal divergence along the boundary but is invalid in many cases having large vertical motion along physical boundaries, such as up–welling in coastal ocean regions (Li et al., 2006) or strong orographic ascent in the atmosphere. Lynch (1989) proposed a three–component partitioning into nondivergent, irrotational, and harmonic flow, while Li et al. (2006) made the two-component decomposition unique by introducing a constraint to the inversion problem that implicitly determines the boundary condition by minimizing the joint amplitude of ψ and ϕ.

774 Here we are concerned with domain boundaries created by the intersection of a
775 pressure surface with topography, with the pressure surface lying at a sufficiently high
776 altitude that the boundaries surround relatively small holes in the otherwise global,
777 spherical domain. Unlike the regional atmospheric model problem in which ψ and
778 ϕ are obtained in a subdomain of global, nonzero atmospheric flow, we know that
779 no wind exists outside of our domain (i.e. beneath Earth's surface). We thus follow
780 the suggestion of Morse and Feshbach (1953) and set the total wind outside the do-
781 main boundaries to zero and invert $\vec{u}$ to obtain unique distributions of ψ and ϕ in
782 the unbounded global domain. Some reanalyses (e.g. ERA-Interim) extrapolate winds
783 beneath Earths surface, so our choice involves replacing those extrapolated values with
784 $\vec{u} = 0$. This choice results in nonzero values of the nondivergent and irrotational wind
785 beneath Earths surface; these two components sum to zero in that region. This con-
786 trasts with methods that assumed nondivergent flow along the boundaries (Watterson,
787 2001), because we recognize that winds can horizontally converge along the topographic
788 boundary at the grid scale of the data; such convergence is common along the Himalaya
789 and Arakan mountains in the summer monsoon. An important point is that our choice
790 of $\vec{u}$ beneath Earths surface, or equivalently of the boundary condition for ψ, has only
791 minor effects on our numerical identification of vortices because that choice alters ψ
792 only by addition of a function with zero curvature, and our identification algorithm
793 involves finding local minima (i.e. regions of positive curvature) in the discretized
794 streamfunction.

Appendix B LPS detection program

796 The command line syntax to obtain LPS tracks from a six-hourly dataset using
797 for TempestExtremes is:

```
798  #candidate searching; $infile is the netcdf file containing input variables.
799
800  ./DetectNodes  --in_data  $infile --out $candidatefile
801  --searchbymin "PSI" --mergedist 5.0
802  --closedcontourcmd "PSI,12.5e5,10,0"
803  --outputcmd "PSI,min,0;msl,min,3;RH,avg,3;zhi,max,2;lsm,max,0;
804      _VECMAG(u10,v10),max,3;msl,minix,3.0"
```

```
805  #Sticting candidates to make track
806  ./StitchNodes --in $candidatefile --out $outfile
807  --format "i,j,lon,lat,strf850,slp,rh,zhi,lsm,sp,minmslix"
808  --range 3.0 --minlength 5 --maxgap 2
809  --threshold "zhi,<=,8000.,4;rh,>=,85,4"
```

```
810  # Calculating some derived quantities using track data
811  #$mslfile is the netcdf file containing mean sea level pressure and surface wind.
812  ./NodeFileEditor --in_file $outfile --out_file $trackfile
813  --in_data $mslfile
814  --in_fmt "lon,lat,strf850,slp,rh,zhi,lsm,sp,minmslix"
815  --calculate "deltaslp=max_closed_contour_delta(msl,10,minmslix);
816      acepsl=eval_acepsl(msl,10.0);
817      ace=eval_ace(u10,v10,3.0);
818      pdi=eval_pdi(u10,v10,3.0);
819      ike=eval_ike(u10,v10,3.0)"
820  --out_fmt "lon,lat,strf850,slp,deltaslp,sp,rh,zhi,lsm,acepsl,ace,pdi,ike"
```

References

Bengtsson, L., Böttger, H., & Kanamitsu, M. (1982). Simulation of hurricane-type vortices in a general circulation model. *Tellus*, *34*(5), 440–457.

Berry, G. J., Reeder, M. J., & Jakob, C. (2012). Coherent synoptic disturbances in the Australian monsoon. *Journal of Climate*, *25*(24), 8409–8421.

Bollasina, M., & Nigam, S. (2009). Indian Ocean SST, evaporation, and precipitation during the South Asian summer monsoon in IPCC-AR4 coupled simulations. *Climate Dynamics*, *33*(7-8), 1017.

Boos, W., Hurley, J., & Murthy, V. (2015). Adiabatic westward drift of Indian monsoon depressions. *Quarterly Journal of the Royal Meteorological Society*, *141*(689), 1035–1048.

Broccoli, A., & Manabe, S. (1990). Can existing climate models be used to study anthropogenic changes in tropical cyclone climate? *Geophysical Research Letters*, *17*(11), 1917–1920.

Chavas, D. R., Reed, K. A., & Knaff, J. A. (2017). Physical understanding of the tropical cyclone wind-pressure relationship. *Nature Communications*, *8*(1), 1–11.

Cohen, N. Y., & Boos, W. R. (2014). Has the number of Indian summer monsoon depressions decreased over the last 30 years? *Geophysical Research Letters*, *41*(22), 7846–7853.

Dee, D. P., Uppala, S., Simmons, A., Berrisford, P., Poli, P., Kobayashi, S., . . . others (2011). The ERA-Interim reanalysis: Configuration and performance of the data assimilation system. *Quarterly Journal of the Royal Meteorological Society*, *137*(656), 553–597.

Delgado, S., Landsea, C. W., & Willoughby, H. (2018). Reanalysis of the 1954–63 Atlantic hurricane seasons. *Journal of Climate*, *31*(11), 4177–4192.

Di Luca, A., Evans, J. P., Pepler, A., Alexander, L., & Argüeso, D. (2015). Resolution sensitivity of cyclone climatology over eastern Australia using six reanalysis products. *Journal of Climate*, *28*(24), 9530–9549.

Ebita, A., Kobayashi, S., Ota, Y., Moriya, M., Kumabe, R., Onogi, K., . . . others (2011). The Japanese 55-year reanalysis JRA-55: an interim report. *Sola*, *7*, 149–152.

Gelaro, R., McCarty, W., Suárez, M. J., Todling, R., Molod, A., Takacs, L., . . . others (2017). The Modern-Era Retrospective Analysis for Research and Applications, Version 2 (MERRA-2). *Journal of Climate*, *30*(14), 5419–5454.

Godbole, R. V. (1977). The composite structure of the monsoon depression. *Tellus*, *29*(1), 25–40.

Hagen, A. B., Strahan-Sakoskie, D., & Luckett, C. (2012). A Reanalysis of the 1944–53 Atlantic Hurricane Seasons—The first Decade of Aircraft Reconnaissance. *Journal of Climate*, *25*(13), 4441–4460.

Hersbach, H., Bell, W., Berrisford, P., Horányi, A., J., M.-S., Nicolas, J., . . . Dee, D. (2019). Global reanalysis: goodbye ERA-Interim, hello ERA5. , 17-24. Retrieved from https://www.ecmwf.int/node/19027 doi: 10.21957/vf291hehd7

Hersbach, H., & Dee, D. (2016). ERA5 reanalysis is in production, ECMWF Newsletter 147, ECMWF. *Reading, UK*.

Hodges, K. I. (1995). Feature tracking on the unit sphere. *Monthly Weather Review*, *123*(12), 3458–3465.

Hodges, K. I. (1998). Feature-point detection using distance transforms: Application to tracking tropical convective complexes. *Monthly Weather Review*, *126*(3), 785–795.

Houze Jr, R., Rasmussen, K., Medina, S., Brodzik, S., & Romatschke, U. (2011). Anomalous atmospheric events leading to the summer 2010 floods in Pakistan. *Bulletin of the American Meteorological Society*, *92*(3), 291–298.

Hunt, K. M., Turner, A. G., Inness, P. M., Parker, D. E., & Levine, R. C. (2016). On the structure and dynamics of Indian monsoon depressions. *Monthly Weather Review*, *144*(9), 3391–3416.

Hurley, J. V., & Boos, W. R. (2015). A global climatology of monsoon low-pressure systems. *Quarterly Journal of the Royal Meteorological Society*, *141*(689), 1049–1064.

India Meteorological Department. (2011). *Tracks of cyclones and depressions over North Indian Ocean (from 1891 onwards), Tech. Note Version 2.0.* Cyclone Warning and Research Centre India Meteorological Department Regional Meteorological Centre, Chennai, India.

Jadhav, S., & Munot, A. (2009). Warming SST of Bay of Bengal and decrease in formation of cyclonic disturbances over the Indian region during southwest monsoon season. *Theoretical and Applied Climatology*, *96*(3-4), 327–336.

Kobayashi, S., Ota, Y., Harada, Y., Ebita, A., Moriya, M., Onoda, H., . . . others (2015). The JRA-55 reanalysis: General specifications and basic characteristics. *Journal of the Meteorological Society of Japan. Ser. II*, *93*(1), 5–48.

Krishnamurthy, V., & Ajayamohan, R. (2010). Composite structure of monsoon low pressure systems and its relation to Indian rainfall. *Journal of Climate*, *23*(16), 4285–4305.

Krishnan, R., Ayantika, D., Kumar, V., & Pokhrel, S. (2011). The long-lived monsoon depressions of 2006 and their linkage with the Indian Ocean Dipole. *International Journal of Climatology*, *31*(9), 1334–1352.

Landsea, C. W., Glenn, D. A., Bredemeyer, W., Chenoweth, M., Ellis, R., Gamache, J., . . . others (2008). A reanalysis of the 1911–20 Atlantic hurricane database. *Journal of Climate*, *21*(10), 2138–2168.

Landsea, C. W., Hagen, A., Bredemeyer, W., Carrasco, C., Glenn, D. A., Santiago, A., . . . Dickinson, M. (2014). A reanalysis of the 1931–43 Atlantic hurricane

database. *Journal of climate*, *27*(16), 6093–6118.

Li, H., Chen, W., & Shen, I.-F. (2006). Segmentation of discrete vector fields. *IEEE Transactions on Visualization and Computer Graphics*, *12*(3), 289–300.

Lynch, P. (1988). Deducing the wind from vorticity and divergence. *Monthly Weather Review*, *116*(1), 86–93.

Lynch, P. (1989). Partitioning the wind in a limited domain. *Monthly Weather Review*, *117*(7), 1492–1500.

Manganello, J. V., Cash, B. A., Hodges, K. I., & Kinter, J. L. (2019). Seasonal forecasts of North Atlantic tropical cyclone activity in the North American multi-model ensemble. *Climate Dynamics*, *53*(12), 7169–7184.

McCarty, W., Coy, L., Gelaro, R., Huang, A., Merkova, D., Smith, E., ... Wargan, K. (2016). MERRA-2 input observations: Summary and assessment. *NASA Tech. Rep. Series on Global Modeling and Data Assimilation, NASA/TM-2016-104606*, *46*, 64.

Michaelis, A. C., & Lackmann, G. M. (2019). Climatological Changes in the Extratropical Transition of Tropical Cyclones in High-Resolution Global Simulations. *Journal of Climate*, *32*(24), 8733–8753.

Mooley, D. A. (1973). Some aspects of Indian monsoon depression and associated rainfall. *Monthly Weather Review*, *101*, 271–280.

Mooley, D. A., & Shukla, J. (1987). *Characteristics of the westward-moving summer monsoon low pressure systems over the Indian region and their relationship with the monsoon rainfall.* University of Maryland, Department of Meteorology, Center for Ocean-Land .

Morse, P., & Feshbach, H. (1953). *Methods of Theoretical Physics [Vol 1-2].*

Pedersen, K. (1971). Balanced systems of equations for the atmospheric motion- A numerical experiment, and an analytical discussion(Linearized two level model for atmospheric motion equations systems, using Psi-balanced system for 24 hour forecast). *Geofysiske Publikasjoner(Geophysica Norvegica)*, *28*, 1–12.

Prajeesh, A., Ashok, K., & Rao, D. B. (2013). Falling monsoon depression frequency: A Gray-Sikka conditions perspective. *Scientific Reports*, *3*, 2989.

Praveen, V., Sandeep, S., & Ajayamohan, R. (2015). On the relationship between mean monsoon precipitation and low pressure systems in climate model simulations. *Journal of Climate*, *28*(13), 5305–5324.

Rácz, Z., & Smith, R. K. (1999). The dynamics of heat lows. *Quarterly Journal of the Royal Meteorological Society*, *125*(553), 225–252.

Rajendra Kumar, J., & Dash, S. (2001). Interdecadal variations of characteristics of monsoon disturbances and their epochal relationships with rainfall and other tropical features. *International Journal of Climatology*, *21*(6), 759–771.

Ramage, C. S. (1971). *Monsoon meteorology (international geophysics series; v. 15).* Academic Press.

Ramanathan, V., Chung, C., Kim, D., Bettge, T., Buja, L., Kiehl, J., ... Wild, M. (2005). Atmospheric brown clouds: Impacts on South Asian climate and hydrological cycle. *Proceedings of the National Academy of Sciences*, *102*(15), 5326–5333.

Rastogi, D., Ashfaq, M., Leung, L. R., Ghosh, S., Saha, A., Hodges, K., & Evans, K. (2018). Characteristics of Bay of Bengal monsoon depressions in the 21st century. *Geophysical Research Letters*, *45*(13), 6637–6645.

Rayner, N., Parker, D. E., Horton, E., Folland, C. K., Alexander, L. V., Rowell, D., ... Kaplan, A. (2003). Global analyses of sea surface temperature, sea ice, and night marine air temperature since the late nineteenth century. *Journal of Geophysical Research: Atmospheres*, *108*(D14).

Saha, S., Moorthi, S., Pan, H.-L., Wu, X., Wang, J., Nadiga, S., ... others (2010). The NCEP climate forecast system reanalysis. *Bulletin of the American Meteorological Society*, *91*(8), 1015–1058.

Saji, N., Goswami, B., Vinayachandran, P., & Yamagata, T. (1999). A dipole mode in the tropical Indian Ocean. *Nature*, *401*(6751), 360.

Sandeep, S., Ajayamohan, R., Boos, W. R., Sabin, T., & Praveen, V. (2018). Decline and poleward shift in Indian summer monsoon synoptic activity in a warming climate. *Proceedings of the National Academy of Sciences*, *115*(11), 2681–2686.

Sanders, F. (1984). Quasi-geostrophic diagnosis of the monsoon depression of 5–8 July 1979. *Journal of the Atmospheric Sciences*, *41*(4), 538–552.

Sangster, W. E. (1960). A method of representing the horizontal pressure force without reduction of station pressures to sea level. *Journal of Meteorology*, *17*(2), 166–176.

Sikka, D. (1978). Some aspects of the life history, structure and movement of monsoon depressions. In *Monsoon dynamics* (pp. 1501–1529). Springer.

Sikka, D. (2006). *A study on the monsoon low pressure systems over the Indian region and their relationship with drought and excess monsoon seasonal rainfall.* Center for Ocean-Land-Atmosphere Studies, Center for the Application of Research on the Environment.

Thorncroft, C., & Hodges, K. (2001). African easterly wave variability and its relationship to Atlantic tropical cyclone activity. *Journal of Climate*, *14*(6), 1166–1179.

Truong, C., Oudre, L., & Vayatis, N. (2019). Selective review of offline change point detection methods. *Signal Processing*, 107299.

Ullrich, P. A., & Zarzycki, C. M. (2017). TempestExtremes: A framework for scale-insensitive pointwise feature tracking on unstructured grids. *Geoscientific Model Development*, *10*(3), 1069.

Vishnu, S., Francis, P., Shenoi, S., & Ramakrishna, S. (2016). On the decreasing trend of the number of monsoon depressions in the Bay of Bengal. *Environmental Research Letters*, *11*(1), 014011.

Vishnu, S., Francis, P. A., Shenoi, S. C., & Ramakrishna, S. S. V. S. (2018). On the relationship between the Pacific Decadal Oscillation and monsoon depressions over the Bay of Bengal. *Atmospheric Science Letters*, *19*(7), e825.

Watterson, I. (2001). Decomposition of global ocean currents using a simple iterative method. *Journal of Atmospheric and Oceanic Technology*, *18*(4), 691–703.

Webster, P. J., Moore, A. M., Loschnigg, J. P., & Leben, R. R. (1999). Coupled ocean–atmosphere dynamics in the Indian Ocean during 1997–98. *Nature*, *401*(6751), 356.

Xavier, P. K., Marzin, C., & Goswami, B. (2007). An objective definition of the Indian summer monsoon season and a new perspective on the ENSO–monsoon relationship. *Quarterly Journal of the Royal Meteorological Society*, *133*(624), 749–764.

Yoon, J.-H., & Chen, T.-C. (2005). Water vapor budget of the Indian monsoon depression. *Tellus A*, *57*(5), 770–782.

Zarzycki, C. M., Thatcher, D. R., & Jablonowski, C. (2017). Objective tropical cyclone extratropical transition detection in high-resolution reanalysis and climate model data. *Journal of Advances in Modeling Earth Systems*, *9*(1), 130–148.

Zarzycki, C. M., & Ullrich, P. A. (2017). Assessing sensitivities in algorithmic detection of tropical cyclones in climate data. *Geophysical Research Letters*, *44*(2), 1141–1149.